ingegneria sismica
International Journal of Earthquake Engineering
Anno XLIII - Num. 3 - 2026

Optimization of Mechanical Properties and Engineering Application Paradigms for High-Durability Masonry Structure Reinforcement Technologies

Qingyi Chen[1,*]

[1] Fujian Provincial Key Laboratory of Bamboo Resources Development and Utilization Sanming University, Sanming 365000, Fujian, China

SUMMARY: *For solving the not matching problem between early mechanical promotion and long-time use stability in masonry reinforcement, this research has established a durability-mechanics linked optimization frame and an engineering use mode for high-durability modification systems. A unified database containing 186 open experimental specimens and 426 constrained parametric cases was organized for masonry walls, spandrels, and arch members. Heterogeneous environmental actions, including freeze-thaw, wet-dry chloride exposure, and thermal cycles, were transformed into an equivalent exposure index to enable cross-study comparison. Based on peak shear strength, displacement ductility, residual capacity retention, equivalent energy dissipation, normalized cost, and construction interference, a coupled performance index was established and used in surrogate-based multi-objective optimization. Results indicate that G-CRM and B-TRM outperform CFRP and SRG in the combined evaluation of initial resistance and durability retention. Under unified exposure conditions, G-CRM attained a peak shear stress of 0.66 MPa and held 0.88 of its capacity before exposure, while B-TRM displayed the maximum drift capacity of 1.19%. The analysis of sensitivity makes known that interface bonding coefficient and anchoring effect efficiency are the main controlling factors of coupling response, therefore the sum of their contribution degrees exceeds 56%. Compared with empirical scheme selection, the Pareto-optimal solutions improve the coupled index by 17.6% with only a 6.3% increase in normalized cost. Finally, a scenario-based decision map is proposed for heritage masonry, occupied coastal housing, and masonry arch bridges, providing differentiated strengthening paradigms centered on compatibility, durability retention, and deployment constraints.*

KEYWORDS: *masonry structures; high-durability strengthening; tRM/CRM; durability-mechanics coupling; engineering application paradigm*

1 Introduction

Existing masonry structures still account for a significant proportion of urban renewal, historic building preservation, and the maintenance of small-to-medium-span transportation infrastructure. In past times, many great quantities of brick-constructed residential houses, stone-constructed public constructions, religious buildings and masonry arch bridges were built by people, which have the characters that original seismic design standards are limited and material change is very big. After long-term service, they have been continuously subjected to the combined effects of wet-dry cycles, salt intrusion, temperature fluctuations, and occasional

*17350538875@163.com
https://doi.org/10.65102/is20261052
Published: 10 June, 2026

fires. Problems encountered at construction sites typically involve not just the propagation of a single crack, but the simultaneous accumulation of multiple forms of deterioration, such as mortar softening, localized spalling, reduced overall stiffness, insufficient shear capacity, and frequent subsequent repairs.Consequently, the requirements for reinforcing such structures are subject to significant engineering constraints: on the one hand, it is necessary to enhance load-bearing capacity and deformation capacity within limited intervention thickness and an acceptable construction schedule; on the other hand, disturbances to the original masonry materials, the building's operational condition, and its visual texture must be minimized. Especially in ancient buildings and currently lived-in dwelling buildings, construction convenience, material matching ability, and long-time firmness are often as important as the early effect promotion.

As for the reaction to these restrictions, the central point of study on masonry strengthening methods has had a big change. Early projects put stress on the direct load-carrying enhancements given by high-strength, light-weight materials like FRP, the technical reason being to quickly solve the masonry’s weak points in in-plane shear resistance and out-of-plane stability through comparatively thin reinforcing layers. This approach yields clear results in regular walls and relatively dry environments; however, as applications have shifted from laboratory wall panels to historic stone masonry, infill walls, thick-walled systems, and short-span arch bridges, material compatibility, adaptability to humid environments, and post-fire residual performance have gradually become new limiting factors.Recent studies indicate that the application of mineral-based composite systems-such as TRM, FRCM, CRM, and SRG-based strengthening work for brick buildings still gets increasing attention. One-side strengthening, the mineral base coating materials with high reversibility, edge fixed anchorage, and small-interference construction ways which are specially made for currently working places have hence become the main development orientations in this domain [1-8]. This trend indicates that masonry reinforcement is no longer merely a matter of comparing material strengths, but is gradually shifting toward a comprehensive selection process where mechanical response, environmental tolerance, and engineering deployment are simultaneously constrained.

The current studies already give an important basis for this work, however they also expose a number of shortcomings which directly influence the making of decisions in the engineering domain. First, there are significant variations across different studies in specimen scale, boundary conditions, loading regimes, and environmental exposure methods; results described as "load-bearing capacity enhancement" or "durability improvement" often lack a unified framework for comparison.Some studies employ monotonic diagonal compression and shear, whereas other researchers utilize circulation loads or partial bending-shear connection; environmental surroundings have many kinds, covering freeze-thaw, wet-dry chloride contact, salt mist, heat circulation, and post-fire situation exposure. Due to the lack of a unified equivalent expression, designers find it difficult to determine whether the advantages of a particular scheme in different studies stem from the material itself or from differences in testing protocols and evaluation metrics.Second, existing work has focused more on the initial mechanical gains of a particular type of reinforcement system-such as peak load-bearing capacity, ductility, or energy dissipation-while insufficient attention has been paid to the coupling relationship between residual load-bearing capacity retention after long-term service, interface bond degradation, and anchorage effectiveness.For masonry structures, interface cracking and delamination often occur before the reinforcement materials can fully realize their potential. If one compares only initial peak values while ignoring the retained capacity after exposure, the resulting optimal results are difficult to directly apply to high-durability design [9-13].

Between the research objects and the engineering situations, a relatively big gap still exists.

Although currently existent research contains experiments or case researches on historical walls, single-faced CRM, post-blaze TRM wall plates, residential type classifications, and arch bridge abdomen reinforcing [14-20], the majority of current researches is still limited to individual topics or situations, and there is a lack of a unified application paradigm which can handle conventional conditions including historical architectures, coastal dwelling buildings which are in use, and masonry arch bridges. The real hard problem which the engineering community at present confronts is not what material can obtain the maximum peak property in lab tests, but on the contrary what system is more reliable, practicable, and can maintain long-term efficacy under various exposure levels, construction influence constraints, and maintenance conditions. Only depending on material sorts or single performance indexes to assess design schemes can bring about two obvious biases: First, systems that have high nominal intensity may lose function ahead of time on account of interface worsening under complex environments; Second, the systems that have better compatibility, although they show a little bit lower initial performance increase, hence they keep more stable load-carrying roads and lower expenditure for maintenance in the period of long-time service. To projects that possess clear high-durability goals, these differences directly influence decisions which concern reinforcement layer thickness, anchorage arrangement, construction arrangement, and later examination strategies.

From the angle of research, the increasing stress on systems which are based on minerals is also connected with the working principle of masonry as a base layer. In brick stone work, loads are born together by block pieces, cement bonding seams, and contact surfaces, and the road that carries loads itself shows very obvious non-continuous character. When the reinforcement layer has entered working state, whether the strength of the reinforcing elements can be converted into stable performance promotion at the component level therefore largely depends on crack controlling in the matrix, the continuity of interface combination, and stress diffusion in the anchorage area. Just for this cause, directly taking reinforcement evaluation methods from reinforced concrete or metal structures often cannot accurately depict the real performance change of masonry components under long-term environment influences. The research about high-durability masonry strengthening must solve the coordinate problems among three scales-material, interface, member-therefore this paper discusses durability description, mechanical targets, engineering restrictions inside a united assessment frame framework.

According to this, this article sets up a research framework which takes the core problem of strengthening high-durability brickwork structures as center, it includes unified specimen arrangement, combined durability-mechanics assessment, and suggestions which are made according to actual engineering situations. This research places stress upon three large aspects. First of all, one public database of testing samples is built by us for brick wall bodies, stone wall bodies, filled wall bodies and masonry arch structure components. Heterogeneous environmental influences-such as freeze-thaw circulations, wet-dry chlorine contact, and heat circulations-are changed into a unified equal exposure measuring norm to solve the problem of cross comparison between different research works. Second, based upon strength, ductility, and residual load-bearing ability, this research brings in cost and construction disturbance restrictions to establish a durability-mechanics coupling index which is suitable for selecting masonry reinforcement plans. Therefore, sensitivity analysis and multi-objective optimization are utilized by us to ascertain the critical ranges of parameters. Third, regarding three classic situations-ancient architecture, in-use coastal dwelling buildings, and stone arch bridges-we put forward adaptation rules and arrangement modes for strengthening systems, thus providing directly usable decision standards for the engineering use of high-durability blockwork structures.

2 Research on Collaborative Optimization of Reinforcement for High-Durability Masonry Structures

2.1 Organization of Test Samples and Equivalent Durability Characterization

The study first addresses the issues of scattered sample sources, inconsistent testing standards, and the inability to directly compare durability conditions.To ensure that subsequent evaluations are based on comparable data, this paper uses publicly published masonry reinforcement tests as the baseline samples, retaining only studies that simultaneously meet the following conditions: First, the test specimens can be clearly identified as brick walls, stone walls, infill walls, masonry lintels, or masonry arch members;Second, the literature provides verifiable material parameters, geometric dimensions, loading regimes, and key responses; third, at least two of the following performance indicators can be extracted: load-bearing capacity, deformation capacity, or post-exposure residual performance. Literature that reports only material-layer performance without component-level responses, provides incomplete descriptions of boundary conditions, or reuses the same test data is excluded from the main sample database.Based on these criteria, a total of 186 basic samples were compiled, including 102 sets of brick masonry walls, 38 sets of stone masonry walls, 18 sets of partition walls and lintels, and 28 sets of masonry arches and infill members.To improve coverage of the parameter space, this study supplemented the base samples with 426 constrained extended cases within the variable boundaries of the base samples, resulting in a total of 612 analysis cases, which were subsequently used uniformly for training, validation, and engineering solution search. The summary of the data is shown in Table 1.

Table 1: Database composition and equivalent exposure settings

Category	Samples	Main Variables	Purpose
Public tests on brick masonry walls	102	$(f_m,\ \tau_0,\ \rho_f,\ t_r,\ \beta_b,\ s_a)$	Primary modeling samples
Public tests on stone masonry walls	38	$(f_m,\ \tau_0,\ \rho_f,\ t_r,\ \beta_b,\ N_e q)$	Compatibility and brittleness checks
Public tests on spandrel walls / lintels	18	$(\tau_0,\ \rho_f,\ t_r,\ s_a, I)$	Local seismic scenarios
Public tests on masonry arches / spandrels	28	$(f_m,\ \rho_f,\ t_r,\ \beta_b,\ N_e q)$	Infrastructure scenarios
Extended cases with constrained parameters	426	$(\rho_f,\ t_r,\ \beta_b,\ s_a,\ N_e q, C, I)$	Sensitivity analysis and optimization
Total	612	—	—

The key to standardizing the sample lies in bringing the objects, variables, and responses from different studies into the same coordinate system. To this end, this paper organized the raw data in four steps. The first step involved standardizing geometric and material parameters by converting wall thickness, net shear area, reinforcement ratio, render thickness, connector arrangement, masonry compressive strength, and mortar joint shear strength into the same dimensional or dimensionless expressions;The second step standardized the loading response metrics, extracting peak load, yield displacement, ultimate displacement, post-peak decline slope, and equivalent energy dissipation for diagonal compression-shear, monotonic horizontal loading, and cyclic in-plane tests;Step 3: Standardize interface information by converting

interface characteristics described in the literature-such as ultimate bond stress, slip transition point, anchor spacing, or edge fixation type-into the interface bond factor βb and anchorage spacing s_a;Step 4: Standardize the expression of environmental exposure by incorporating freeze-thaw, wet-dry-chloride, and thermal cycling into a single durability characterization for subsequent comparison and optimization. The organizational structure of features after public samples are entered into the database and their mapping to downstream tasks are shown in Figure 1.

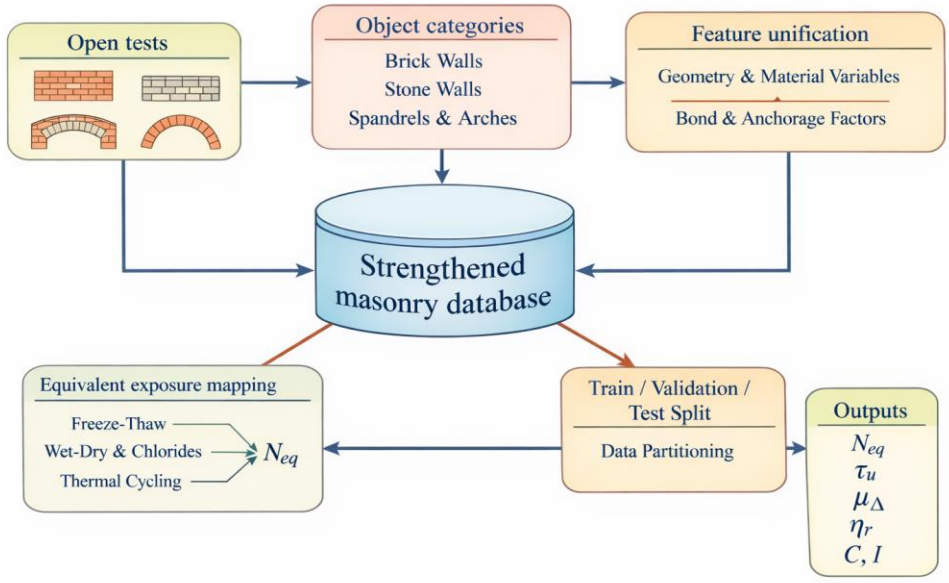

Figure 1: Database organization and equivalent exposure mapping for strengthened masonry.

To convert heterogeneous exposure conditions into comparable durability variables, this paper converts different environmental actions into equivalent exposure cycles and uses this quantity as the unified durability input in the database. The expression is shown in Equation (1).

$$N_{eq} = \lambda_1 N_{ft} + \lambda_2 N_{wd} + \lambda_3 N_{th} \tag{1}$$

where: N_{eq} represents the equivalent exposure cycle; N_{ft} denotes the number of freeze-thaw cycles; N_{wd} denotes the number of wet-dry chloride cycles; N_{th} denotes the number of thermal cycles; λ_1 ,λ_2, and λ_3 are conversion factors representing the influence of different exposure pathways on residual performance. This study uses the retrievable residual load decay slope from published tests as the calibration basis to uniformly convert the three types of environmental actions, enabling exposure levels from different literature sources to be projected onto the same coordinate axis.The purpose of this approach is not to eliminate differences in the mechanisms of environmental effects, but to provide a unified metric for cross-comparison. After conversion, the distribution range of the base sample's N_{eq} is 0-300, where 0-100 primarily corresponds to mild service damage, 100-220 corresponds to moderate exposure, and values above 220 correspond to conditions involving sustained humid heat, salt, or thermal cycling.

After we carry out the standardization work on the durability variables, this research then goes on to arrange the training, validation and test data sets. Because the proportion of brick masonry samples is very high, stratified sampling method was utilized in order that the model would not be controlled by a single kind of specimen: 70% was assigned to the training set, 15% to the validation set, and 15% to the test set, and at the same time consistent proportions are

kept in both the specimen type dimension and the exposure level dimension. As for load-displacement curves which have a small quantity of missing middle data points, the present study has utilized piecewise cubic interpolation for the reconstruction of the envelope; With regard to outlier data points, they have been eliminated by employing a threshold which is 1.5 times the interquartile range of tests that belong to the same type. All continuous variables are undergone minimum-maximum normalization before they enter the surrogate model, and discrete construction variables are expressed as dummy variables. Table 1 gives in presentation the database composition, variable groupings, and classification of usages. After finishing the above processing, the originally scattered data which came from different testing systems have been compressed into a data space that can be compared, thus this provides a foundation which can be reused for the coupled evaluation that comes afterwards.

2.2 Mechanical-Durability Coupled Evaluation and Parameter Optimization

After the sample organization was completed, this paper further addressed how to evaluate the relative merits of reinforcement schemes under a unified standard.Comparing only peak load-bearing capacity would exaggerate the short-term advantages of certain high-modulus materials while neglecting the impact of interface degradation and construction disturbances on long-term service performance. Based on this consideration, this paper incorporates peak shear capacity, residual load-bearing retention, displacement ductility, normalized cost, and construction disturbances into the evaluation system, and uses a single coupled index to reflect the comprehensive performance of the schemes.For each sample group, the peak shear stress τ_u, residual load retention η_r, displacement ductility μ_Δ, normalized cost C, and construction disturbance index *I* are first extracted from experiments or extended case studies. Subsequently, each indicator is converted to the 0-1 range to eliminate dimensional differences.

After standardizing the metrics, this study adopts the durability-mechanical coupling performance index J as the core criterion for subsequent parameter screening and Pareto search. Its expression is shown in Equation (2).

$$J = \omega_1 \bar{\tau}_u + \omega_2 \bar{\eta}_r + \omega_3 \bar{\mu}_\Delta - \omega_4 \bar{C} - \omega_5 \bar{I} \tag{2}$$

where, J is the coupled performance index; $\bar{\tau}_u$ is the normalized peak shear stress; $\bar{\eta}_r$ is the normalized residual load-bearing capacity; $\bar{\mu}_\Delta$ is the normalized displacement ductility; $\bar{C}$ is the normalized cost; $\bar{I}$ is the normalized construction disturbance index; and ω_1 to ω_5 are the respective weights.Given that the subject of this paper is oriented toward high-durability applications, the weight settings place greater emphasis on load-bearing capacity retention and long-term effectiveness. This configuration ensures that the evaluation of schemes is not dominated by a single strength indicator, while simultaneously preserving the constraining effect of construction and economic constraints on the results. The relationship between the durability-mechanics coupled index and the control variables is shown in Figure 2.

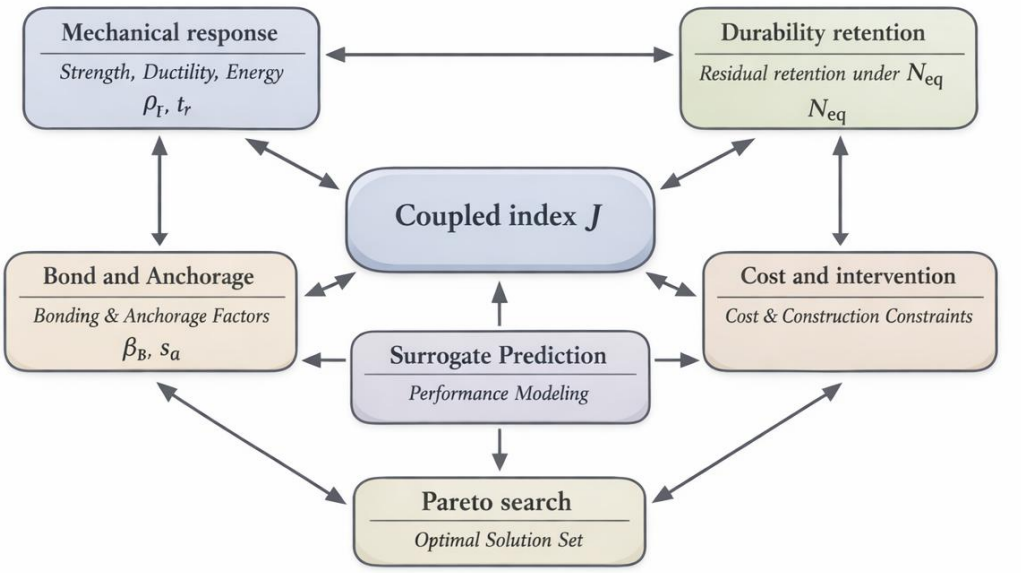

Figure 2: Coupled evaluation and parameter optimization of high-durability masonry strengthening schemes.

To solve the problem of J , this paper adopts a technical approach that combines variable screening, surrogate prediction, and multi-objective search.First, the parameters most relevant to masonry reinforcement were selected from the 10 design variables, including the reinforcement ratio ρ_f, render thickness t_r, interface bond factor β_b , anchorage spacing s_a, post-cracking ductility parameters of the matrix, connector stiffness, masonry compressive strength f_m, initial shear resistance τ_0, equivalent exposure cycles $N_e q$, and construction constraint level.Subsequently, a Sobol global sensitivity analysis was employed to identify dominant variables and reduce the dimensions of subsequent searches.In the parameter exploration phase, Latin hypercubic sampling was used to generate constrained scenarios, with constraint boundaries derived from the variable distributions of published experiments and common engineering values, ensuring that the expanded cases remained within feasible ranges. Compared to methods that only interpolate near experimental points, this approach is better suited for finding robust solutions under constrained conditions rather than pursuing extreme solutions that are theoretically possible but difficult to implement in practice.

In the part of surrogate model building, forecasting devices are set up separately for peak shear stress, remaining capacity keeping ratio, and displacement ductility. Because the sample size is not big and variables have nonlinear mutual connections, this research uses an overall prediction framework that puts gradient-boosted regression and Gaussian process regression together: the previous one catches high-order nonlinear connections between variables, therefore the latter one makes correction for smoothness and uncertainty in local areas. In the training stage, five-fold cross-validation is utilized by the authors, the evaluation measurement items contain the coefficient of determination R^2, the mean absolute percentage error, and the residual distribution of the verification dataset. If the verification residual errors for a specific output are systematically big for a certain category of objects, therefore the system goes back to the sample level to re-check the input dimensions and influence factors for that category. This two-direction checking forms a closed-loop connection between data arrangement and model study, hence decreasing wrong judgments that come from sample difference in properties.

Once the surrogate model achieves stable predictive capability, this paper further performs multi-objective optimization. The optimization objective is not merely to maximize the J , but to find a set of non-inferior solutions while satisfying engineering constraints.For historic

building scenarios, additional hard constraints include thickness, material compatibility, and surface reversibility; for coastal residential buildings in service, hard constraints include single-sided constructability, work area occupancy time, and resistance to salt and moisture; for masonry arch bridges, hard constraints include crack control in tension zones, ease of inspection, and the feasibility of edge anchoring. In this way, the model no longer outputs abstract optimal parameters, but rather candidate solutions that can be directly translated into engineering decisions across different scenarios. This paper treats interface bonding and anchorage efficiency as primary control factors, and the enhanced modulus of elasticity and reinforcement layer thickness as secondary control factors. This approach stems from the load-bearing characteristics of masonry members: when the interface cannot stably transfer forces, increasing the strength of the material itself is unlikely to translate into long-term gains at the member level; conversely, once interface continuity is ensured, moderate thickness and appropriate reinforcement often yield more robust overall performance.

2.3 Validation Strategy and Engineering Adaptation Criteria

In the research verification procedure, the ultimate mission is to prove that the above-mentioned framework can both explain current experiment outcomes and give guidance to practical engineering suggestion proposals. For this purpose, this paper builds a two-level verification flow on the data level and the component level. Data-level verification concentrates on the generalization ability of the substitute model, which uses stratified five-fold cross-validation and one independent test collection to check prediction mistakes among different object kinds, exposure regions and reinforcement systems. Component-level verification includes establishing finite element models of typical brick walls, stone walls, and arch bridge web components to carry out back-calibration comparisons for peak loads, limit displacements, and interface slipping. In the finite element models, the masonry body adopts a damage-plastic constitutive model, the render layer utilizes layered shell elements, the reinforcement is simulated through equivalent embedded bars, and the interface uses a tensile-separating bond element. In addition, the decrease of stiffness is brought in the anchorage area to reflect the sliding and partial relaxing of real fasteners. By this method, the verification at component level may directly correspond to the failure positions of highest sensitivity in experiments, hence it does not only give out overall errors of load bearing.

After completing the model validation, this paper further transforms the comprehensive performance criteria into executable selection rules for engineering scenarios. Considering that the same J value may have different implications across different projects, this paper introduces a scenario-adaptive score S_k, which incorporates comprehensive performance, historical compatibility, operational interference, and maintenance convenience into the recommendation criteria. Its expression is shown in Equation (3).

$$S_k = \beta_1 J_k + \beta_2 H_k + \beta_3 U_k + \beta_4 M_k \tag{3}$$

In the equation, S_k represents the scenario adaptation score for the k th candidate scheme; J_k is the coupling performance index for the corresponding scheme; H_k is the historical compatibility score; U_k is the controllability of usage interference score; M_k is the maintenance convenience score; and β_1 to β_4 are the scenario weights.For historic buildings, β_2 is assigned a higher value to emphasize material compatibility and surface reversibility; for occupied residential buildings, β_1 and β_3 are given greater weight to balance performance and construction duration; for arch bridge components, the weights of β_1 and β_4 are increased to highlight long-term service life and inspection convenience. With this

configuration, the model's recommended logic shifts from a uniform ranking to a scenario-specific ordering.

The establishment of scenario scores does not rely on subjective descriptions but corresponds to a set of quantifiable criteria. Historical compatibility is calculated based on differences in the elastic modulus of the substrate, material permeability, and surface coating thickness; construction interference is scored based on single- or double-sided construction, duration of wet work, and curing time; and maintenance convenience is determined by a combination of the ease of visual inspection, accessibility for localized repairs, and corrosion resistance of fasteners.Each sub-score is first normalized to the 0-1 range and then combined with scenario-specific weights to form the S_k. The closed-loop relationship between model validation and engineering decision-making is illustrated in Figure 3.

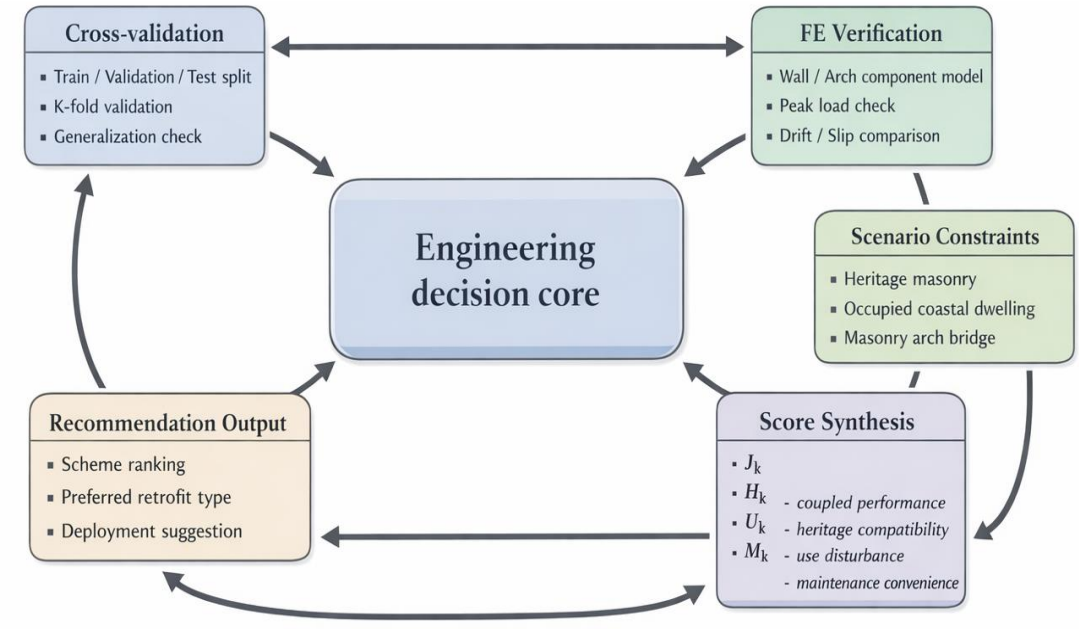

Figure 3: Closed-loop validation and scenario-oriented decision protocol for masonry strengthening.

Through this closed-loop process, this paper not only identifies which reinforcement systems perform better statistically but also explains why this advantage holds in specific engineering scenarios, under what conditions it diminishes, and when it is necessary to shift from high strength to high robustness.

3 Analysis of Reinforcement Effects and Engineering Adaptability for High-Durability Masonry Structures

3.1 Load-bearing and Durability Retention Characteristics of Different Reinforcement Systems

After completing the standardization of samples and establishing a coupled evaluation framework, Table 2 summarizes the differences in load-bearing capacity, deformation, and durability retention among different strengthening systems under the same evaluation criteria.

Table 2: Mechanical and Durability Performance of Different Strengthening Systems

System	(τ_u)/ MPa	Limit Drift/ %	Normalized Energy Dissipation (E_d)/-	Residual Retention Rate (η_r)/-	Stiffness Retention Rate/-	Normalized Cost/-	Construction Disturbance/-
CFRP	0.59	0.95	1.32	0.74	0.72	1.00	0.43
B-TRM	0.64	1.19	1.81	0.86	0.83	0.86	0.36
G-CRM	0.66	1.14	1.67	0.88	0.85	0.91	0.31
SRG	0.61	1.05	1.49	0.82	0.79	0.95	0.38

The response differences among various reinforcement systems under uniform monotonic shear-compression loading are shown in Figure 4.

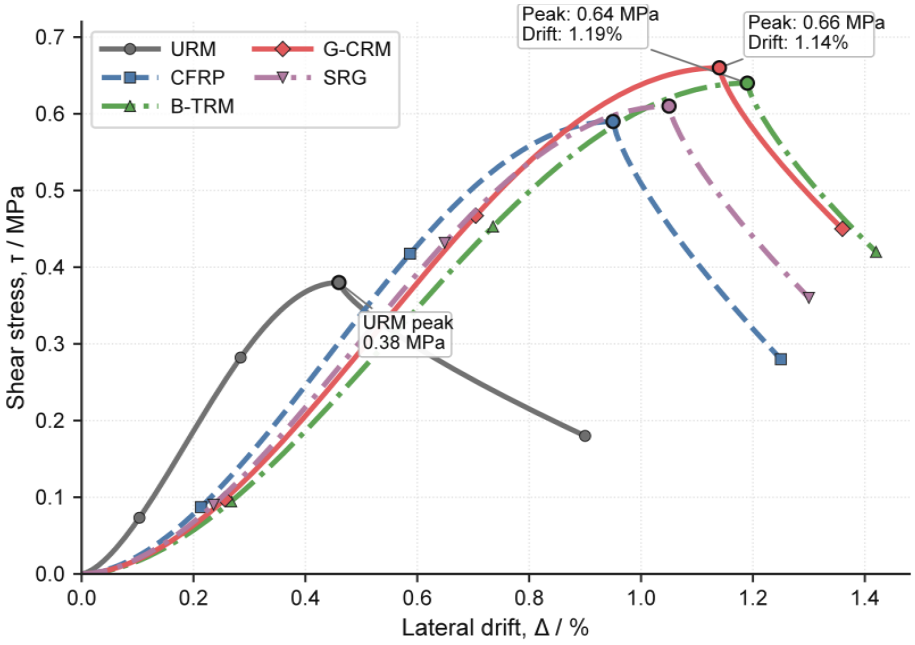

Figure 4: Envelope curves of strengthened masonry under monotonic shear-compression loading.

In terms of initial load-bearing capacity and deformation capacity, the mineral-based systems exhibit a more balanced improvement. The peak shear stress of the URM reference wall is 0.38 MPa, with a limit drift of 0.46%. After CFRP reinforcement, the peak shear stress increases to 0.59 MPa, representing a 55.3% increase, and the limit drift increases to 0.95%;B-TRM and G-CRM reached 0.64 MPa and 0.66 MPa, respectively, corresponding to increases of 68.4% and 73.7%, with ultimate drifts of 1.19% and 1.14%, respectively; the peak shear stress of SRG was 0.61 MPa, with an ultimate drift of 1.05%.In Figure 4, the post-peak decay phase for B-TRM and G-CRM is longer, indicating that the mineral-based matrix can maintain a relatively continuous load-transfer path even after cracking in the base layer; the post-peak decay for CFRP is steeper.

The energy dissipation characteristics further illustrate this difference. Using the normalized energy dissipation of URM (1.00) as a reference, CFRP, B-TRM, G-CRM, and SRG reached 1.32, 1.81, 1.67, and 1.49, respectively. B-TRM exhibited the highest increase in energy dissipation, indicating that the ductile lime matrix possesses better strain redistribution capability in the post-cracking stage;G-CRM's peak load is slightly higher than that of B-TRM,

but its energy absorption is slightly lower, indicating that its advantages primarily lie in overall confinement and load-bearing capacity. In terms of the average softening slope after the peak, B-TRM and G-CRM show reductions of 39.5% and 34.8% compared to URM, respectively, while SRG shows a reduction of 22.6% and CFRP only 14.7%.When analyzing residual performance after environmental exposure, the differences between the various systems become even more pronounced. The residual load-bearing retention patterns after exposure are shown in Figure 5.

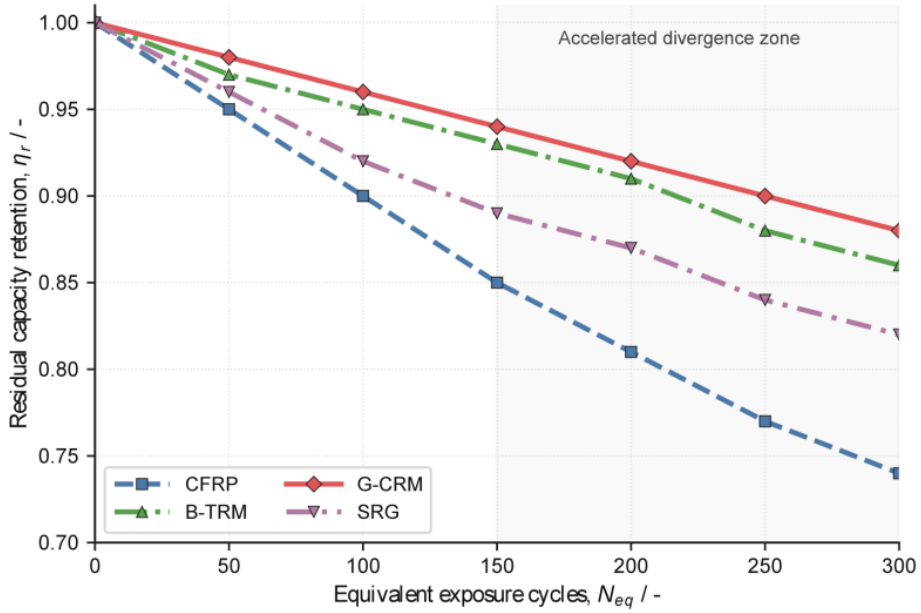

Figure 5: Residual capacity retention versus equivalent exposure cycles.

Figure 5 demonstrates the residual load-bearing capability retention percentages after 0 to 300 equivalent exposure cycles. When Neq equals 100, the CFRP, B-TRM, G-CRM and SRG have decreased to 0.90, 0.95, 0.96 and 0.92, in order respectively; When N_{eq} is 150, the values are 0.85, 0.93, 0.94 and 0.89, each one in order; and when N_{eq} reaches 300, they have a further decrease to 0.74, 0.86, 0.88, and 0.82. In Figure 5, the descent gradient of CFRP rises greatly after 150 equal exposures, this shows that its interface connection is more easy to have accumulative degrading under the together functions of heat, wetness, and salt. On the opposite side, the curves of B-TRM and G-CRM have a slower descending trend, which indicates that the stiffness matching between the mineral-base base material and the masonry underlayer, together with the interface vapor permeability, is more helpful for keeping the long-term structural completeness. As what Table 2 summarizes, G-CRM has obtained the maximum numerical values for the three index items of peak shear stress, residual strength reservation, and stiffness reservation, which are 0.66 MPa, 0.88, and 0.85, each; in the aspect of displacement ductility and energy dissipation ability, B-TRM obtained the best performance, the corresponding values are 1.19% and 1.81, respectively. It is very obvious that for projects which need a balance between service-life stability and constructability, the selection standards ought to change from short-term peak strength to the combined function of load-bearing capacity, deformation capability, and residual retention.

Table 2: Comparison of generation quality on the CelebA dataset

Network framework	Image generation resolution	Inception Score
PGGAN	128×128	10.12
The proposed(γ=0.5)	128×128	12.43
The proposed(γ=0.7)	128×128	11.75
The proposed(γ=0.9)	128×128	10.46
PGGAN	256×256	5.34
The proposed(γ=0.5)	256×256	9.25
The proposed(γ=0.7)	256×256	8.31
The proposed(γ=0.9)	256×256	7.58

3.2 Analysis of Ablation Experiments

After confirming the overall performance of different systems, this section further analyzes the key parameters of the dominant high-durability reinforcement scheme and their optimization benefits. The combined effect of the interface bond factor and reinforcement ratio on the coupled performance index is shown in Figure 6.

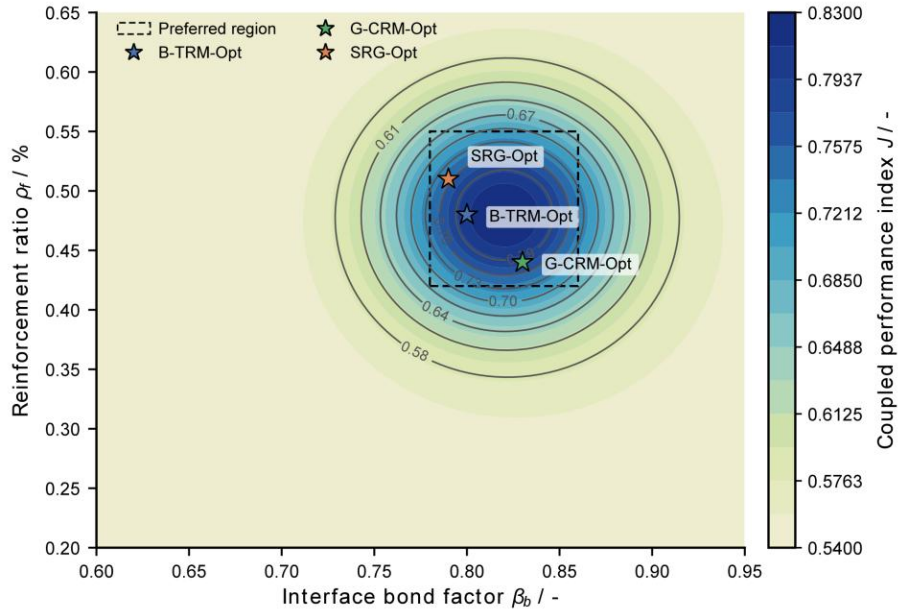

Figure 6: Response heatmap of the coupled performance index as a function of bond factor and reinforcement ratio.

Figure 6 illustrates the combined effect of the interface bond factor β_b and the reinforcement ratio ρ_f on the coupled performance index J. The high-value regions are primarily concentrated within the ranges of β_b = 0.78-0.86 and ρ_f = 0.42%-0.55%, indicating that a higher reinforcement ratio does not necessarily yield better results.Whenρ_f is increased from 0.30% to 0.48%, if β_b is simultaneously maintained at around 0.80,J can be increased from 0.67 to

0.84; however, whenρ_f continues to increase to 0.62% while β_b remains below 0.72, J drops back to 0.79. This indicates that an excessively high reinforcement ratio transfers more constraint demands to the interface and edge anchorage zones.Sobol sensitivity analysis indicates that the contribution rates are as follows: β_b accounts for 31.4%, anchorage efficiency for 24.7%, post-cracking ductility of the matrix for 18.9%, reinforcement ratio for

14.2%, screed thickness for 6.1%, and modulus of the reinforcement for 4.7%. The first two items combined account for more than half of the total, making the interface and anchorage primary control variables. Based on the aforementioned response patterns, this study further performs a Pareto search. The cost-performance non-dominant solution distributions for different candidate schemes are shown in Figure 7.

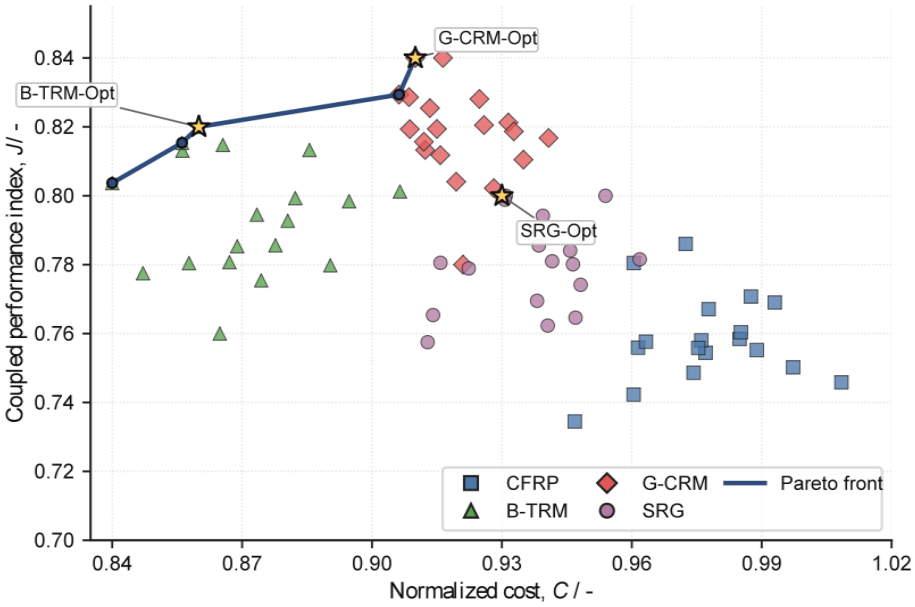

Figure 7: Pareto front of normalized cost and coupled performance.

In Figure 7, non-dominant solutions are primarily distributed within the intervals of normalized cost 0.84-0.98 and coupling performance index 0.78-0.84.Compared to the average values of the empirical solution library, the Pareto-optimal solution achieves a 17.6% improvement in the J, an 8.9% increase in residual load retention, a mere 6.3% increase in normalized cost, and an 11.2% reduction in construction disturbance.Among the specific solutions, B-TRM-Opt achieves an$J$ of 0.82 with a combination of ρ_f = 0.48%, t_r = 24 mm, and s_a = 240 mm, making it more suitable for projects with high compatibility requirements; G-CRM-Opt reaches an$J$ of 0.84 at ρ_f = 0.44%, t_r = 28 mm, and s_a = 220 mm, positioning it at the top of the Pareto front and making it the candidate solution with the most stable overall performance;SRG-Opt achieves J = 0.80 with a thinner layer, remaining attractive under scenarios with limited additional thickness and tensile zone control. In contrast, simply increasing thickness does not enter the frontier region, indicating that the core of high-durability optimization lies not in using more material, but in ensuring that the interface, anchorage, and reinforcement configuration are in a matched state.

The dependability of the optimization outcomes must also be supported by the model's accuracy and the analysis of errors. The R^2 numerical values of the substitute model in five-time cross-validation were: peak shearing stress 0.913, displacement ductility 0.887, residual load holding 0.901, and energy consumption 0.876; On the independent test set, the average absolute percentage errors, respectively, were 7.1%, 8.6%, 7.4%, and 9.2%. If every one among 426 groups of expanded cases is searched one by one with member-grade finite elements, therefore the total time it needs is approximately 3.8 hours; however, when we use the surrogate model, a parameter scanning of the same scale was finished within 12.4 seconds. In the verification of component level, the average error of peak load was 6.8%, the average error of limit drift was 8.5%, and the peak error of interface slip was 7.9%. The mistakes mainly came from non-uniformities in documented boundary compression stress and loading speeds, the lack

of starting conditions for fastening parts, and the hardship of completely describing interface microcracks which are brought by long-time exposure through using one single equal parameter.

3.3 Analysis of Typical Application Scenarios and Engineering Deployment

The foregoing two sections have discussed what kinds of systems have higher overall stability and which parameters deserve priority control; this section in addition gives these conclusions to particular engineering situations. Figure 8 gives a scene dividing on basis of exposure strength and intervention limit conditions, while Table 3 makes a summary of marking outcomes and suggested schemes for three typical target kinds. To historic masonry walls, the control conditions mainly come from material matching, reversibility, and the thickness of surface processing measures.

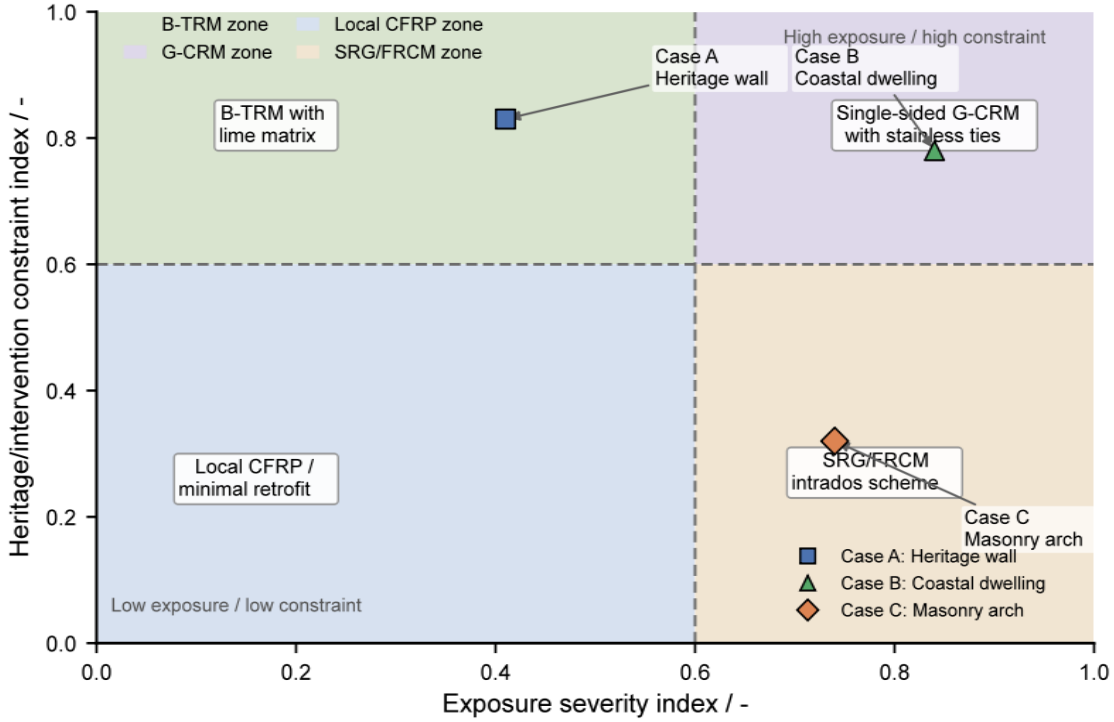

Figure 8: Scenario-oriented application map for masonry strengthening paradigms.

In Figure 8, the solutions that people prefer for zones with high past sensitivity are concentrated upon the side which uses lime-based B-TRM. From Table 3 we can see, B-TRM has obtained a suitability assessment score of 0.82 inside this situation, which is higher than 0.76 that G-CRM gets and 0.63 that CFRP gets. Its strong points come from the little rigidity difference between the lime-based base body and the already existing mortar seams, the capacity of the 22-25 mm thin-layer processing to control surface covering area, and the gradual after-cracking behavior that better keeps the original structure load-bearing features. Hence, the comprehensive performance of B-TRM is better than that of solutions which have lower compatibility.

Table 3: Scenario suitability scores and recommended application paradigms

Scenario	Key Constraints	Recommended Paradigm	Adaptation Score (S_k)	Residual Retention Rate (η_r)	Construction Disturbance/-	Engineering Implications
Historical Masonry Wall	High Compatibility, Reversible, Controlled Thickness	Lime-based B-TRM + Peripheral Anchoring	0.82	0.89	0.28	Preserves permeability and crack relief capacity
Coastal In-Service Brick Residential	High Salt Wet Exposure, One-Sided Construction, Shortened Construction Period	One-Sided G-CRM + Stainless Steel Connectors	0.84	0.91	0.24	Balances long-term durability and construction accessibility
Masonry Arch Bridge Soffit	Tension Zone Control, Easy Inspection, Thin Layer Reinforcement	SRG/FRCM Soffit Strips + Edge Anchoring	0.80	0.87	0.34	Increases safety reserves and controls crack width

For the current brick-masonry residential buildings which are located in coastal regions, the emphasis is transferred to the conditions of high salt content, humid environment, only one side can be approached, and the construction period is relatively short. Under this group of constraint conditions, the most superior solution mainly is located in the one-sided G-CRM plan. In Table 3, it can be seen that G-CRM has obtained a scenario score which is 0.84, a residual retention rate which is 0.91, and a construction disturbance index which is 0.24. This outcome is in accordance with its material and building features: the one-sided CRM system reduces to the smallest extent the taking up of residents' living space, and the combined restriction which is formed by metal connecting pieces and mineral-based mortar is more suitable for keeping long-term load transmission in wet surroundings. When compared with the double-sided mineral-base covering plan, the one-side G-CRM is able to cut down the time length that work space is taken up by 23%, hence it still keeps a remaining load-carrying ability of around 0.90 in zones that have high exposure.

For the soffits of masonry arch bridges and similar tension-controlled members, the focus lies on thin-layer confinement, crack control, and ease of inspection.In Table 3, the suitability score for the SRG/FRCM inner surface scheme is 0.80, higher than the 0.74 for B-TRM. This is because the critical zones in such members are more concentrated in the inner surface tension zone; when the reinforcement is directly placed along the tension path, it can provide more direct structural reinforcement with a smaller additional thickness.The scenario analysis in this paper indicates that, provided edge anchoring is reliable, the SRG/FRCM scheme can increase the safety margin for arch bridge service conditions by 32%, reduce service crack width by 37%, and make it easier to identify local damage locations during subsequent inspections.

Through overall analysis of three kinds of situations, we can find that the engineering application mode that this paper puts forward obeys a clear division of labor logic. To the historic buildings, in which compatibility and surface controllability are put on the first place, the lime-based B-TRM is the choice that people prefer; for coastal residence constructions that are currently being used, wherein durable performance keeping and single-face building work are laid stress on, G-CRM is the better choice; and regarding arch bridges and members

controlled by local tension, for which thin-layer tension reinforcing bars and convenience for inspection are the key points, SRG/FRCM is the option that people prefer to choose. Although CFRP did not stand in the first ranks in the evaluation of high durability, it still can act as an alternative choice for fast partial reinforcement under dry environment conditions and strict thickness restrictions.

4 Conclusion

This current paper has discussion on the engineering demands that relate to the reinforcing work of masonry buildings with high durable ability. It has built a research framework that couples durability with mechanics, which faces toward scheme selection and scenario arrangement, therefore finishes comparisons of different reinforcement systems, parameter optimization, and engineering suitability analysis within a unified sample range. This research points out that the choosing standards for brick masonry reinforcement work cannot be restricted only to the promotion of the initial load-bearing ability, but also need to take into account the keeping of residual capacity, interface stability, interference in construction work and matching degree of use scenarios.

(1) This present article has constructed a unified specimen system that includes brick wall bodies, stone wall bodies, infill wall bodies, and masonry arch component parts. It has brought together 186 groups of publicly open test samples and 426 groups of limited expanded cases into one sole database. Through using equal exposure circulation periods, this research realizes an unified expression of different durability situations, therefore it gives a repeatable data basis for cross contrast of high-durability masonry reinforcement work.

(2) In terms of methodology and results, the durability-mechanical coupling performance index proposed in this paper can simultaneously characterize load-bearing capacity, ductility, residual capacity retention, cost, and construction interference. The results show that G-CRM performs most consistently in peak load-bearing capacity and durability retention, while B-TRM has advantages in deformation capacity and energy dissipation;compared to empirical schemes, the Pareto-optimal solution achieves a 17.6% improvement in comprehensive performance, an 8.9% increase in residual load retention, and keeps the cost increase within 6.3%. Further sensitivity analysis indicates that interface bonding and anchorage efficiency are primary control factors for high-durability design.

(3) On the level of engineering application, this article sets up different deployment patterns for old buildings, coastal house structures that are being used, and masonry arch bridges: lime-based B-TRM is put first for old masonry; The single-sided G-CRM has more suitability for coastal dwelling constructions; and SRG/FRCM schemes can be put in first position for arch bridge components that have obvious tensile control situations. The insufficiencies of this research contain the inadequate consideration of long-term creep, fastener rust, and the combined influences of multiple kinds of disasters. Further consummation of exposure drawing and scenario weight calculation needs to be carried out by means of long-term observation and large-scale demonstration projects.

Funding

Fujian Provincial Key Laboratory of Bamboo Resource Development and Utilization, B170002, KCP2503

References

[1] Hafner, I., Kišiček, T., & Gams, M. (2023). Review of methods for seismic strengthening of masonry piers and walls. Buildings, 13(6), 1524.

[2] Kouris, L. A. S., & Triantafillou, T. C. (2018). State-of-the-art on strengthening of masonry structures with textile reinforced mortar (TRM). Construction and Building Materials, 188, 1221-1233.

[3] Gattesco, N., Rizzi, E., Boem, I., et al. (2023). A new method of seismic strengthening stone masonry with CRM coatings on one side. Construction and Building Materials, 407, 133565.

[4] Gams, M., Boem, I., Gattesco, N., et al. (2024). Experimental study on the seismic enhancement of brick masonry spandrels using a single-sided composite reinforced mortar coating. Bulletin of Earthquake Engineering, 22, 2531-2552.

[5] Liapopoulou, M., Bompa, D. V., & Elghazouli, A. Y. (2024). In and out of plane behaviour of TRM strengthened heritage masonry elements. Construction and Building Materials, 448, 138152.

[6] Alecci, V., Fagone, M., Galassi, S., et al. (2024). Experimental shear behaviour of masonry walls reinforced with FRCM. Engineering Structures, 315, 118425.

[7] Estevan, L., Torres, B., Baeza, F. J., et al. (2023). Masonry walls strengthened with textile reinforced mortars (TRM) and subjected to in-plane cyclic loads after real fire exposure. Engineering Structures, 296, 116922.

[8] Illampas, R., Rigopoulos, I., & Ioannou, I. (2024). Development and performance evaluation of a novel high-ductility fiber-reinforced lime-pozzolana matrix for textile reinforced mortar (TRM) masonry strengthening applications. Materials and Structures, 57, 75.

[9] Azimi, N., Oliveira, D. V., Schollbach, K., et al. (2025). Durability and bond behavior of textile-reinforced mortar composites under prolonged saline exposure. Journal of Building Engineering, 112, 113887.

[10] Çelik, A., Mercimek, Ö., Akkaya, S. T., et al. (2025). A novel bond-slip model between TRM strips and different types of masonry walls: Experimental approach. Construction and Building Materials, 458, 139595.

[11] Çelik, A., Mercimek, Ö., Anıl, Ö., et al. (2025). Bond-slip models for textile reinforced mortar strengthened masonry walls. Engineering Structures, 343, 121263.

[12] Gattesco, N., Rizzi, E., Boem, I., et al. (2025). Seismic strengthening of existing brick masonry with CRM coatings on one side. Bulletin of Earthquake Engineering, 23(9), 3779-3808.

[13] Kallioras, S., Bournas, D., Koutas, L., et al. (2024). Integrated seismic and energy retrofitting of masonry-infilled RC buildings with textile-reinforced mortar and thermal insulation: Full-scale tests on a five-story prototype. Journal of Building Engineering, 98,

111006.

[14] Petrovčič, S., Prašnikar, P., & Kilar, V. (2025). Seismic assessment and FRCM strengthening of post-war masonry residential buildings: A case study on building typologies. International Journal of Disaster Risk Reduction, 119, 105341.

[15] Zampieri, P., Piazzon, R., Santinon, D., et al. (2025). Intrados FRCM-strengthening of a masonry bridge: Experimental and analytical investigations. Engineering Structures, 323, 119215.

[16] Mavros, M., Hadjipantelis, N., Ioannou, I., et al. (2025). In-plane strengthening of heritage masonry structures using 3D-printed steel reinforcement: Experimental proof-of-concept. Construction and Building Materials, 499, 143746.

[17] Fares, S., Meriggi, P., De Santis, S., et al. (2025). Experimental investigation on the tensile and bond durability of galvanized steel reinforced grout. Buildings, 15(17), 3020.

[18] Askouni, P. D., Kapsalis, P., Papanicolaou, C. G., et al. (2025). Strengthening of masonry and concrete members with textile-reinforced alkali-activated mortars: A review on the mechanical performance. Materials, 18(7), 1517.

[19] Majumder, A., Stochino, F., Valdes, M., et al. (2025). Sustainable masonry retrofitting and upgrading techniques: A review. Fibers, 13(6), 68.

[20] D'Antino, T. (2025). Advances and open issues in the use of fiber-reinforced composites as reinforcement of existing and new constructions. Materials and Structures, 58, 312.

[21] Angiolilli, M., Gregori, A., Pathirage, M., et al. (2020). Fiber reinforced cementitious matrix (FRCM) for strengthening historical stone masonry structures: Experiments and computations. Engineering Structures, 224, 111102.

[22] Dalalbashi, A., Ghiassi, B., & Oliveira, D. V. (2021). A multi-level investigation on the mechanical response of TRM-strengthened masonry. Materials and Structures, 54(6), 224.

[23] Wang, X., Lam, C. C., & Iu, V. P. (2019). Comparison of different types of TRM composites for strengthening masonry panels. Construction and Building Materials, 219, 184-194.

[24] Ismail, N., & Ingham, J. M. (2016). In-plane and out-of-plane testing of unreinforced masonry walls strengthened using polymer textile reinforced mortar. Engineering Structures, 118, 167-177.

[25] Papanicolaou, C. G., Triantafillou, T. C., Karlos, K., et al. (2007). Textile-reinforced mortar (TRM) versus FRP as strengthening material of URM walls: In-plane cyclic loading. Materials and Structures, 40(10), 1081-1097.